

A language-inspired machine learning approach for solving strongly correlated problems with dynamical mean-field theory

Hovan Lee,¹ Zelong Zhao,² George H. Booth,² Weifeng Ge,^{3,*} and Cedric Weber^{2,†}

¹*Department of Physics, Royal Holloway, University of London, Egham, TW20 0EX, United Kingdom*

²*King's College London, Theory and Simulation of Condensed Matter (TSCM), The Strand, London WC2R 2LS, UK*

³*Nebula AI Group, School of Computer Science, Fudan University*

We present SCALINN — Strongly Correlated Approach with Language Inspired Neural Network — as a method for solving the Anderson impurity model and reducing the computational cost of dynamical mean-field theory calculations. Inspired by the success of generative Transformer networks in natural language processing, SCALINN utilizes an in-house modified Transformer network in order to learn correlated Matsubara Green's functions, which act as solutions to the impurity model. This is achieved by providing the network with low-cost Matsubara Green's functions, thereby overcoming the computational cost of high accuracy solutions. Across different temperatures and interaction strengths, the performance of SCALINN is demonstrated in both physical observables (spectral function, Matsubara Green's functions, quasi-particle weight), and the mean squared error cost values of the neural network, showcasing the network's ability to accelerate Green's function based calculations of correlated materials.

I. INTRODUCTION

Widespread interest has been devoted in the last three decades to strongly correlated materials, which are being used in emerging technologies, such as spintronics, quantum computing and high temperature superconductivity for example. They are characterised by strong electronic interactions between their d and f -band valence electrons. The interplay between electron itinerancy (quasi-particle behavior) and electron-electron Coulomb interactions (Mott physics) provides a challenge for standard electronic theories, such as density function theories. These two energy scales overlap for strongly correlated systems, and therefore, the problem cannot be simplified as the perturbative expansion of one property against the static backdrop of another. The competing effects of itinerancy and interaction-induced localization necessitates treating these properties on equal footing.

In the past decades significant progress in understanding the underlying physics of strong electron correlation effects has been made by the dynamical mean-field theory (DMFT) method [1–3], in particular with the harnessing of DMFT to widespread materials modelling methods, such as density functional theory (DFT), with the DFT+DMFT combined approach [4–6] [7], notably in research into high temperature superconductivity [8–10], cold-atom optical trapping [11–13], and topologically ordered phases [14–16] among others. In short, DFT+DMFT leads to structural and energetic predictions which are key for material research, which is especially important when sampling large spaces of structures with structural relaxations.

Despite this formidable achievement, practical challenges remain with the DFT+DMFT approach. At

the heart of the theory is the choice of the quantum engine that solves the many-body Anderson Impurity Model (AIM), an underlying model that provides the local Green's function of the compound of interest via a self-consistent mapping. [17] [18, 19]. In this scheme, the object to be converged is the Green's function: the descriptor of creation, propagation, and subsequent annihilation of an electron or hole in a many-body interacting system.

Various methods have been developed to calculate the Green's functions of the AIM within the self-consistent cycle of a DMFT calculation. However, each of these solvers have their own limitations. Examples of these solvers include:

The Hubbard-I (HI) solver [7], which assumes no electron itinerancy, and is therefore an approximation that is only reasonable for highly localized systems.

The iterative perturbation theory (IPT) solver [17] and its third order extension, which contains all first, second (and optionally third) order irreducible diagrams in the proper self energy. This is an accurate solver in the low correlation regime, but does not generalize well beyond systems that are half-filled and relatively low interaction strength.

Continuous time quantum Monte Carlo (CTQMC) methods [20–23] splits the Hamiltonian of the system into two parts (generally hybridization or interaction), and expands the full partition function as powers of one such part, where these powers are stochastically sampled. While formally exact, this method is nonetheless burdened with the sign problem, random errors, and the requirement to analytically continue the resulting Green's function.

Finally, the exact diagonalization (ED) solver [24–26] which computes the eigenvalues of the AIM Hamiltonian directly, and without approximation in the physics. However, this approach becomes exponentially prohibitive as an increasing number of impurity or bath orbitals are taken into consideration. This therefore limits the num-

* wfge@fudan.edu.cn

† cedric.weber@kcl.ac.uk

ber of orbitals in the calculation, and introduces a finite bath discretization error of the hybridization into the resulting Green’s function.

While this represents an incomplete list of all DMFT solvers that have been considered to date, it is clear that deficiencies remain, and research into improved AIM solvers is still a highly active area of research.

A potential solution could well emerge from another discipline; machine learning. Due to advancements in hardware accelerators, improvements in memory capacity, and access to increasingly large databases, deep learning has dominated the field of machine learning in the last decade [27–29]. These developments have given hope to materials scientists; methods to overcome long standing bottlenecks in condensed matter may be in reach [30, 31]. A far-from-complete list of these machine learning driven efforts include: predictions of protein structures [32], the learning of exchange-correlation functionals for density functional theory [33], the challenge of ill-conditioned analytic continuation of dynamical quantities [34], or previous efforts aimed at tackling the same problem of DMFT solvers [35–37].

In this work, we develop and demonstrate the capabilities of SCALINN — Strongly Correlated Approach with Language Inspired Neural Network — which is based on the Transformer architecture [29]. SCALINN predicts the Green’s functions of strongly correlated systems as ordered sequences in the Matsubara domain, this is done in order to reliably solve single-impurity Anderson models (SIAM) within self-consistent DMFT calculations. Here, prediction refers to the machine learning terminology of the output of a neural network that has been trained on a dataset.

Rather than encoding the SIAM Hamiltonian directly into the network as input parameters, the characteristics of the SIAM are instead encoded as (potentially multiple) computationally cheap input Green’s functions. Optionally, additional characteristic system parameters are also supplemented to the network input, in order to generate more accurate estimates of the target Green’s function from the decoder.

The Transformer framework was chosen due to: 1) its potentially infinite memory span — Green’s functions as continuous sequential frequency data exhibits non-local dependence between different frequency points, and therefore requires the memory provided by the Transformer network, 2) the parallelism enabled by the Transformer formalism, and 3) in the absence of word embedding, the query, key and value method provides a rich representation between Green’s function frequency sequence entries. Through this method, we find that the Transformer network is able to learn the mapping between these cheap, low-level SIAM input Green’s functions, and the fully correlated output Green’s functions. This enables reliable predictions within DMFT iterations in a non-perturbative manner. 4) the independence of the model on the number of Matsubara points in training, here the number of points is not case specific, in com-

parison to previously attempted methods such as fully connected deep neural networks.

In comparison to other neural networks, a fully connected network or a kernel ridge regression model will only be able to predict series of fixed length. Our model, in contrast, can provide predictions of varying lengths without the need of retraining the model, allowing for the learning of abstract information from the dataset of, and the prediction on, materials with a wide range of characteristic energy scales.

In this work, the high energy tails of the predicted green’s functions will span the space of Hamiltonian parameters spanned in the training data base. The physical regime that is captured by many-body effects is at low frequency. Here, the method provides a natural pathway to all intermediate regimes between the Fermi liquid phenomenon (frequencies below the coherence temperature), and the single electron picture at high energy. We outline a natural framework that provides a systematic approach to this problem.

The performance of SCALINN at different values of temperature and interaction strengths is showcased in this work, along with predictions of spectral functions, quasi-particle weights and Matsubara Green’s functions. More technical parameters, including training and testing errors of the network across different hyperparameters are given in the supplementary material. Once the machine learning model has been trained to a satisfactory accuracy (to be defined in section II.B.), the run-time computational cost is independent of the complexity of the problem. We report improvements over the team’s previous machine learning DMFT solver [36]. In particular, SCALINN is able to predict the Green’s function of the Hubbard model at inverse temperature $\beta = 100$ (the energy range at which low energy excitation occurs) across various values of Coulomb interaction U with a mean squared error (MSE) of $\sim 10^{-7}$, enabling the prediction of the self energy and spectral function of the system. This is a significant improvement from the previous attempt which was able to reach a validation loss of $\sim 10^{-3}$ at $\beta = 50$, which was shown to be able to calculate the quasi-particle weight of the system, but was unable to provide predictions on the self energy and spectral function.

II. RESULTS

A. Computational Details

To setup the training data of the model, three $G^{\text{ED}}(i\omega_n)$ data-sets at different inverse temperatures of $\beta = 10, 50, 100$ were generated, each consisting of 14,000 different 7-bath SIAM Hamiltonians. The ED Green’s functions were generated using the ED-KCL package [51], with DMFT functionality where required enabled via interface to the TRIQS package [38]. Implementation of the Transformer model made use of the PyTorch pack-

age [52]. The training of our base model, detailed in Table A1, was conducted on a single NVIDIA A100 GPU, where each model was trained on 80% of the data for 350,000 steps, which took approximately 9 hours per model, with the rest of the data used for evaluation of the model accuracy. During run-time, each DMFT loop takes $\sim 10^3$ seconds on the A100 GPU. It should be noted that this GPU computational cost is independent on the number of bath orbitals of the training dataset. In contrast, a traditional 7-bath orbitals ED calculation on the same GPU takes ~ 1 minute, the size of the Green's function matrix to be inverted (as shown in Fig. 4) scales as 2^N for a paramagnetic calculation, and as such the computational cost of each ED DMFT loop scales accordingly.

The bath parameters of the SIAM for these data-sets were calculated as approximations to a continuous semi-circular spectral hybridization,

$$\Delta^{\text{Bethe}}(i\omega_n) = \frac{1}{2\pi^2} \int_{-\infty}^{\infty} d\omega \frac{\sqrt{W^2 - \omega^2}}{i\omega_n - \omega} \Theta(W - |\omega|), \quad (1)$$

with bandwidth $2W$. This hybridization represents the paradigmatic Bethe lattice, which represents an exact model for DMFT [18], with physical hybridizations of relevance to the applicability of DMFT expected to be close to this form. The different 7-bath Hamiltonian parameters were found by initializing the parameters randomly, and subsequently minimizing the error in the effective hybridization of the model (Eq. 8) via changes in V_p and ϵ_p according to

$$\sum_{i\omega_n} \frac{1}{i\omega_n} (\Delta^{\text{bath}}(i\omega_n) - \Delta^{\text{Bethe}}(i\omega_n))^2. \quad (2)$$

This fit is constraint to ensure that particle-hole symmetry of the bath parameters is maintained (with one bath energy constrained to $\omega = 0$), and is stopped early when the squared error in the fit reaches only $1W$, in order to provide the different Hamiltonians. To complete the definition of the SIAM, U values are uniformly generated in the range 0-10 W .

The impurity level ϵ_d is kept at $-U/2W$, and the chemical potential μ is set to $-\epsilon_d - U/2W$. Where these values were chosen to ensure consideration of the particle-hole symmetric point of these Hamiltonians. When demonstrating the use of SCALINN as a solver in a DMFT calculation, the self-energy of Eq. 10 is self-consistently updated, with the interactions able to induce significant changes to the approximately semi-circular initial spectrum, including metal-insulator phase transitions.

B. Truncated Hamiltonian

We first consider the ‘truncated’ mode of operation of the SCALINN model, whereby predictions of the 7-bath SIAM models are created from ED Green's functions with only 3 bath orbitals, mitigating the exponential increase in cost of ED with respect to bath size. The

3-bath SIAM Hamiltonians were created from their 7-bath counterparts by inclusion of the $\epsilon = 0W$ bath orbital, and then selection of one particle-hole symmetric pair of bath orbitals at finite frequency. This allows us to create three 3-bath SIAM approximations to each SIAM of interest. These are solved with ED to provide the input to SCALINN, as described in Sec. IV B.

An example of the effect that this bath dropout has on Green's functions is shown in Fig. 1.a, where these truncated bath models differ significantly from the desired 7-bath solution. Unless otherwise specified, $G(i\omega_n)$ indicates only the imaginary component of the Green's functions in all the figures shown below.

SCALINN nevertheless predicts the 7-bath orbitals ED solution with high accuracy after training of the model. SCALINN models are trained at three different inverse temperatures, with the average training error reduced to below $J(\hat{G}(i\omega_n), G^{\text{ED}}(i\omega_n)) < 10^{-5}$ in all cases. We can analytically continue the predicted Matsubara Green's functions onto the real-frequency axis via Padé approximants, to consider their accuracy of the real-frequency spectrum, shown in Fig. 1.b for a representative test-set prediction, with three values of inverse temperature β and three values of interaction U .

The SCALINN predictions agree very well with the ED ground truth for these systems, even on the real axis, with only small deviations are observed in Fig. 1.b. As the interaction increases, classic hallmarks of correlated materials emerge, with low U describing metals with a single quasi-particle peak at zero energy. As temperature increases (or as β decreases), so does the rate of scattering between electrons, leading to a broadening of these peaks. At intermediate interaction strength $U = 3W$, lower and upper Hubbard bands at $\pm U/2W$ emerge around the quasi-particle peaks at $\omega = 0$. Once again, due to increasing rates of scattering, these three sets of peaks are broadened as temperature increases. Lastly, at higher interaction strength still $U = 6W$, the magnitude of the quasi-particle peaks are greatly reduced in favor of the Hubbard bands. However, due to the lack of DMFT self-consistency in this case, the fully insulating Mott solution was not recovered.

C. Hybrid Approximation Solver

In addition to the truncated bath approach, as discussed in Sec. IV B, we also consider a Hubbard-I+IPT hybrid scheme. In this hybrid method, models were trained from a combination of Hubbard-I and IPT approximate solutions to the target SIAM, and used as inputs to the transformer model to predict target ED-quality outputs. Once again, three separate inverse temperature models were trained to reach errors of $J(\hat{G}(i\omega_n), G^{\text{ED}}(i\omega_n)) < 10^{-5}$ across the entire training set.

In Fig. 2, the various Matsubara Green's functions are presented, including the Hubbard-I and IPT inputs, the

ED ground truth and SCALINN prediction. As expected, the Hubbard-I inputs are all insulating solutions, as observed with $G^{\text{HI}}(i\omega_n)$ tending towards zero as $i\omega_n \rightarrow 0$, consistent with its description of the atomic solution. This is increasingly erroneous for lower temperatures and interaction strengths, where delocalized solutions should be found. In contrast, the IPT input favors delocalized descriptions, where all solutions reach a maximum absolute value as $i\omega_n \rightarrow 0$, which is in error particularly for higher interactions in the non-perturbative U/W limit. In contrast to these computationally cheap input models, the SCALINN predictions match the ED results to remarkably high accuracy from these inputs.

Finally, we consider the utility of the scheme as a solver within a fully self-consistent DMFT calculation. In this, the IPT and Hubbard-I approximations can be found in the absence of bath discretization error of the hybridization. Therefore, while the training of the SCALINN model is performed in the presence of the finite bath approximation to the hybridization, its use within a DMFT scheme can aim to eliminate both the bath discretization error, as well as approximations to the correlated effects of approximate solvers. In order to benchmark the accuracy of the approach, we therefore turn to comparison with a CTQMC solver which can obtain correlated Green's functions in the limit of a continuous hybridization via Monte Carlo sampling, as long as the temperature is not too low such that the fermion sign problem manifests.

In Fig. 3, we consider DMFT on the continuous hybridization of the Bethe lattice (Eq. 1) at $\beta = 10$ compared to CTQMC, for both the final self-consistent Matsubara Greens function, and the quasiparticle weight, Z . This quasiparticle weight can be computed as

$$Z = \frac{\text{Im} \{ \Sigma(i\omega_n) \}}{\omega_n} \Big|_{\omega_n \rightarrow 0}, \quad (3)$$

from the converged DMFT self-energy. Values close to unity indicate a metallic solution, with lower values describing the increased effective mass towards a Mott insulating solution. This is observed from the results, with DMFT+SCALINN agreeing almost perfectly with the DMFT+CTQMC renormalization factor, with the DMFT+IPT biasing towards the metallic phase, and DMFT+Hubbard-I the atomic Mott phase.

Moreover, the self-consistent DMFT Matsubara Green's functions with these various solvers are plotted in Fig. 3.b, where as interaction strength increases, the solutions become increasingly insulating, as can be observed from the $i\omega_n \rightarrow 0$ trend of $G(i\omega_n)$, with once again the discrepancy between SCALINN and CTQMC solvers is indistinguishable on the scale of the plot. It should be noted that these insulating solutions differ from the single-shot SIAM solutions of Fig. 2, due to the self-consistent update of the continuous hybridization in the full DMFT scheme.

III. DISCUSSION

With the insights gained from drawing comparisons to natural language processing problems, we developed a novel and promising approach to predict Green's function sequences in the Matsubara domain via modifications to a Transformer model. These predicted sequences exhibit levels of accuracy that were previously restricted to comparatively high computational costs of exact diagonalization. We considered approaches to both predict these Green's functions of general SIAM models from inputs based on results from computationally accessible lower levels of theory, as well as an approach to mitigate the bath discretization error in describing SIAM's with a continuous hybridization spectrum. Finally, we combined these developments in a fully self-consistent DMFT scheme to solve the Bethe lattice Hubbard model with results indistinguishable from exact CTQMC benchmarks.

However, while the approach showcases much potential, there exist remaining challenges to overcome. Firstly, the approach was restricted to a relatively narrow class of SIAM models from a training dataset of a maximum of 7 fermionic levels. This set of training data can still be improved upon to reach competitive levels as a DMFT solver. As such, the extension to multi-impurity, matrix-valued Green's functions and a wider set of representative hybridizations is required. The advantage gained from the use of this model is that once a model is trained from this set of larger number of fermionic levels, wider hybridization representation extended dataset, the run-time GPU computational cost does not increase accordingly. Note however that one of the key take-aways of our work is that sampling the entire space of AIM (those represented by 7-bath orbitals and all those that aren't) is not required to achieve excellent accuracy for the machine learning approach. Essentially our work demonstrates that training the network on discretized AIMs provides a solid network that can apply to any AIMs. One remarkable demonstration is that comparison to the exact (within statistical error bars) CTQMC results for DMFT. Extending the database with AIM with larger bath orbitals has been shown in our work to only provide minor improvements, see for instance the analysis in table A3 in the supplementary information where we review the dependence on number of bath orbitals. Adaptations of the model to *enforce* desirable features such as causality of the output Green's functions or symmetries would be beneficial, and help avoid convergence issues in the self-consistent DMFT loops which manifested at times for low temperatures or quantum phase transitions. Finally, alternative methods to provide training data of exact Green's functions would allow for an extension to overcome the bath discretization which is manifest in the training of the model. Nevertheless, our findings highlight the power and adaptability of the Transformer model within the field of correlated materials and its potential for pushing the frontiers of computational problem-solving in this domain.

IV. METHODS

A. DMFT Primer

The SIAM is defined as:

$$\begin{aligned} \hat{H}_{\text{SIAM}} = & \underbrace{\sum_{i,j,\sigma} (\varepsilon_{ij\sigma} - \mu) \hat{a}_{i\sigma}^\dagger \hat{a}_{j\sigma}}_{\hat{H}_{\text{bath}}} + \underbrace{\sum_{i,\sigma} (V_{i\sigma} \hat{c}_\sigma^\dagger \hat{a}_{i\sigma} + h.c.)}_{\hat{H}_{\text{hyb}}} \\ & + \underbrace{\sum_{\sigma} (\varepsilon_d - \mu) \hat{c}_\sigma^\dagger \hat{c}_\sigma + U \hat{c}_\uparrow^\dagger \hat{c}_\uparrow \hat{c}_\downarrow^\dagger \hat{c}_\downarrow}_{\hat{H}_{\text{imp}}}, \end{aligned} \quad (4)$$

Where the first term \hat{H}_{bath} describes the dispersion of uncorrelated bath electrons of spin state σ and site index i , with their annihilation (creation) operators $\hat{a}_{i,\sigma}^{(\dagger)}$ and chemical potential μ . The second term \hat{H}_{hyb} determines the hybridization between the impurity and the bath electrons, parameterized by the hybridization strength $V_{i\sigma}$. The last term \hat{H}_{imp} characterizes the impurity electrons at impurity energy level ε_d , with creation (annihilation) operators $\hat{c}_\sigma^{(\dagger)}$ and on-site screened Coulomb interaction strength U .

Without the on-site screened Coulomb interaction (setting $U = 0$), the non-interacting total (including both bath and impurity electrons) Green's function of the SIAM is:

$$G_{\text{tot}}^0(i\omega_n) = \frac{1}{i\omega_n + \mu - \begin{bmatrix} \varepsilon_d & \mathbf{V} \\ \mathbf{V}^\dagger & \varepsilon \end{bmatrix}}, \quad (5)$$

where $i\omega_n$ are the Matsubara frequencies and the spin index σ can be dropped as there are no interactions that change the spin state in our consideration. \mathbf{V} is a vector of the hybridization strengths V_i , and ε is a matrix containing the dispersion energies of the uncorrelated bath electrons ε_{ij} .

Although the DMFT procedure can be carried out in real frequency ω , we choose to operate in Matsubara frequency, as this approach does not require artificial broadening and does not introduce sharp features in the Green's functions that destabilize convergence, in line with methods that interface DMFT with DFT such as TRIQS [38], ABINIT [39] and CASTEP [40]. Most of these implementations are performed in the CTQMC Matsubara frequency framework, as such these solvers scale well with the number of orbitals. On this note, numerical renormalization group (NRG) provides a unique toolset to analyze the spectral features of the single band Hubbard model with a remarkable accuracy. As such, NRG has suggested as a solver for DMFT through various machine learning approaches[41–43]. However, it is a notorious challenge to extend NRG to multi-orbital sys-

tems, and a port of call for DFT+DMFT charge self-consistent approaches lies instead with Matsubara based solvers such as quantum Monte Carlo.

The properties of the impurity does not explicitly depend on the details of the dispersion of the non-correlated electrons, or the hybridization strengths, as such the bath information can be condensed and only the top left block of $G_{\text{tot}}^0(i\omega_n)$ need to be examined:

$$G_{\text{imp}}^0(i\omega_n) = \frac{1}{i\omega_n + \mu - \varepsilon_d - \Delta(i\omega_n)}, \quad (6)$$

$$\Delta(i\omega_n) = V_i \left(\frac{1}{i\omega_n + \mu - \varepsilon_{ij}} \right) V_j^*, \quad (7)$$

where $G_{\text{imp}}^0(i\omega_n)$ is the non-interacting impurity Green's function, and is the top left block of $G_{\text{tot}}^0(i\omega_n)$. $\Delta(i\omega_n)$ is the hybridization function, which encapsulates all contributions of the bath electrons to the properties of the impurity. In this project, this hybridization function is approximated with finite bath discretization:

$$\Delta^{\text{bath}}(i\omega_n) \approx \sum_{p=1}^{N_b} V_p^2 / (i\omega_n - \varepsilon_p), \quad (8)$$

with number of bath sites N_b and bath site index p . Each bath site has hybridization strength V_p and energy ε_p . These parameters are typically fit via numerical techniques [44].

In this work, the Green's function of the Hubbard model is self-consistently mapped onto the $G_{\text{imp}}(i\omega_n)$ of an SIAM via the DMFT procedure [19]. That is, the $G_{\text{imp}}(i\omega_n)$ is expressed as the momentum \mathbf{k} -dependent lattice Green's functions of the Hubbard model via: where $N_{\mathbf{k}}$ is the number of \mathbf{k} points taken into consideration.

To include the effects of interactions, the Dyson equation is applied:

$$[G_{\text{imp}}(i\omega_n)]^{-1} = [G_{\text{imp}}^0(i\omega_n)]^{-1} - \Sigma(i\omega_n), \quad (9)$$

The inclusion of these correlation effects modifies the description of the itinerancy in the uncorrelated bath electrons in eq. (4). As a result of this, the correlated Green's function of the SIAM, hybridization function $\Delta(i\omega_n)$ and self-energy $\Sigma(i\omega_n)$ all have to be updated multiple times until self-consistency of these quantities is achieved.

The DMFT loop can then be written self-consistently:

$$\begin{aligned} G_{\text{imp}}(i\omega_n) &= \frac{1}{N_{\mathbf{k}}} \sum_{\mathbf{k}} G_{\mathbf{k}}^{\text{lattice}}(i\omega_n) \\ &= \frac{1}{N_{\mathbf{k}}} \sum_{\mathbf{k}} [i\omega_n + \mu - \varepsilon_{\mathbf{k}} - \Sigma(i\omega_n)]^{-1} \\ &= \frac{1}{N_{\mathbf{k}}} \sum_{\mathbf{k}} [\varepsilon_d + \Delta^{\text{bath}}(i\omega_n) - \varepsilon_{\mathbf{k}} + G_{\text{imp}}(i\omega_n)^{-1}]^{-1}, \end{aligned} \quad (10)$$

where $G_{\text{imp}}(i\omega_n)$ is present on both sides of the equation, and is updated self-consistently at each iteration.

Updating this self-consistent loop until convergence is a well defined but demanding task, and is where the overhead of computational cost sits. Conventionally this task is carried out by the DMFT solver, here SCALINN is applied to approximate the iterative update of $G_{\text{imp}}(i\omega_n)$ with near instantaneous overhead.

B. SCALINN Overview

SCALINN is a version of the original Transformer model by Vaswani et al. [29], modified such that the inputs and output represent series of Matsubara Green's function data. A broad, conceptual explanation of the framework is as follows: The model is auto regressive, meaning that it receives an input Matsubara Green's function sequence $G^{\text{input}}(i\omega_n)$, from which a prediction of the next entry of the sequence $\hat{G}(i\omega_n)$ is made. This additional predicted entry, and all future predictions, are fed back into the model as $G^{\text{aux}}(i\omega_n)$, which is then used to inform the next prediction in the sequence.

That is, as the model generates the predicted Green's function entry-by-entry, it has the ability to reference $G(i\omega_n^{\text{input}})$ and G^{aux} . This property of referencing is called attention, and the amount of attention that each entry in $G(i\omega_n^{\text{input}})$ and G^{aux} is applied towards the prediction of the next entry, is learned by the model through training.

Focusing now on the components of the transformer model, the individual values of $G(i\omega_n^{\text{input}})$ is augmented with information of their Matsubara frequency values through various different methods that are detailed in the supplementary information. This is referred to as Matsubara encoding in Fig. 5. This information is then fed into a multilayer perceptron block, which is a fully connected neuron network. The output of the multilayer preceptron is then fed into the encoder block.

The encoder block maps all input information into an abstract representation, such that self-attention can be applied to the input sequence: self-attention is a method that allows the model to learn the associations between the entries of the input sequence amongst themselves, in our context this relates to the discrete representation of the Green's function in Matsubara frequencies. It is worth noting that there is a natural delineation in frequency space, as for instance the large frequency behavior relates to the underlying Hamiltonian and fermionic statistic, whereas the low energy frequencies relate to the emergence of quasi-particle excitations.

For example, an input prompt of a language model transformer that generates phrases, might be in the form of the string "He was efficient in his work". From this string, the model might learn a high degree of association between the words "He" and "his", and the words "efficient" and "work", whilst the word "was" might be attended to highly by the model predictions in order to

generate sentences which add to the context of why this person is no longer working efficiently.

Typically, here we used a variation of the transformer that was developed in the context of large language models and the framework that is used in all GPT models (see for instance the seminal work of Vaswani et al. [29]). However, note that the exploration of applications of language models to quantum many body systems remains scarce, this is hence a largely unexplored area. In particular, how the hyper-parameters translate to Green's functions is a focus of this work.

The transformer performs self-attention through the use of the query, key and value (QKV) system, which itself is obtained its name from search engine retrieval mechanisms, as such, this process can be understood analogously with a Google scholar search example: A search engine query is compared to the various keys identified by the search engine, these keys might include the title of an academic paper, the year of publication, the publication journal, etc. From these information, the search engine will output a list of the publications that correspond to the highest values that match the queries with the keys.

Note that queries and keys in language models are abstracted into numerical factors that provide an intermediate abstract layer. This provides opportunities for applying this method to various applications outside the scope of language, such as numerical methods used in quantum sciences.

In the transformer encoder described in this manuscript, since the model learns the associations between the entries of $G(i\omega_n^{\text{input}})$ with other entries of $G(i\omega_n^{\text{input}})$, these queries, keys and values are simply three different abstract representations of the input sequence. Moreover, this QKV process can be performed multiple times in parallel, where each parallel module is called a head in the multi-headed attention (MHA) encoder block, and each head can potentially learn information that is different to other heads.

The decoder portion of the model works in a similar manner: G^{aux} entries are augmented with their Matsubara frequency information, and is fed to a multilayer preceptron block. The information is then inputted into a right-shifted target masked MHA block. The name right-shifted target masked comes from the original work on the use of transformers as language models, where words that are generated from the input sequence prompt appears to the right of the prompt (right-shifted). Moreover, when training the model, whether on segments of text or Green's function sequences, databases containing "True" information is applied to the model (a range of grammatically correct text for language models, and Green's functions calculated from exact-diagonalization in our model). Whilst learning, the model should be agnostic to the entries to the right of the prediction. As such, the decoder needs to be right-shifted target masked to prevent the model from relying on information that does not yet exist during run-time.

Lastly, the output of the first MHA of the decoder is supplied together with the output of the MHA of the encoder, to a second block of decoder MHA. This source masked MHA block takes the encoder output as queries and keys, and matches the information to the values of the first decoder MHA in order to predict the next entry of the Green’s function.

We consider two different modes of operation to test the viability and validity of our approach:

In the first, we consider the potential to overcome bath discretization error in ED solvers. Although the ED Green’s function subspace does not capture the entire phase space spanned by all Matsubara Green’s functions, the subspace is uniformly representative, and spans across the metal-insulator transition. This is tested by discarding a number of discretized baths from N-bath orbitals ED system, and hence the bath orbitals are ‘truncated’ (shown in Fig. 5.b). Whilst we have trained models from various different numbers of bath orbitals sites. Due to the computational cost to generate the training datasets, we report our results from a model trained on 7-bath orbitals in the main text, with details and results of the other models in the supplementary information. We report that as the number of bath orbitals used to train the model increases, the accuracy of predictions increases. Given the exponential scaling in calculations with respect to bath size, this method would provide substantial benefit in computational cost. Three of these truncated systems were created, such that all of the 7 bath orbitals from the full system is present in at least one of the truncated systems. This is a similar motivation to the ‘distributed exact diagonalization’ approach [45]. The mapping between the Green’s functions of these truncated systems G_7^{Trunc} and the target Green’s function G^{ED} is then learned by the network. We report that this approach produces Green’s functions that are in agreement with the exact calculations obtained from CTQMC.

The second approach is for the network to learn G^{ED} from input Green’s functions of complementary characteristics. In our attempts, the HI and the IPT solvers were used. These two input models, while computationally cheap, allow for a description of different extremes in correlated physics. Specifically, HI is superior in the atomic limit, while IPT describes the low- U itinerant physics as a perturbative expansion in powers of U . We will denote this approach the ‘hybrid method’.

The cost function to be minimized in the training of both models is defined as the mean squared error to the 7-bath orbitals ED solution at a set of training points,

$$J(\hat{G}(i\omega_n), G^{\text{ED}}(i\omega_n)) = \frac{1}{N} \sum_{n=0}^{N-1} (\hat{G}(i\omega_n) - G^{\text{ED}}(i\omega_n))^2, \quad (11)$$

where $\hat{G}(i\omega_n)$ is the predicted Green’s function, $G^{\text{ED}}(i\omega_n)$ is the 7-bath orbitals ED solution of the SIAM, and the sum is performed over the first $N = 32$ Matsubara frequency points. This value can be increased, such that the model is trained to generate as many Matsub-

ara frequency points as required. In practice, increasing the number of Matsubara points considered in this mean squared error evaluation does not dramatically increase the accuracy of the prediction, as will be shown below, the results obtained from the model is within the statistical error bars of the CTQMC result.

Although the ED solver can calculate Green’s functions directly on the real-frequency axis ω , the choice of working in Matsubara frequency $i\omega_n$ is motivated by the power of the transformer architecture and similarities that $G(i\omega_n)$ — as a Matsubara series — share with word sequences.

Matsubara points are the poles of the Fermi-Dirac function and hence the representation is discrete, akin to words of a sentence. Moreover, $G(i\omega_n)$ is a well-defined analytic function for all Matsubara points at equilibrium, tending to a smooth and differentiable function as the temperature is lowered.

This sequence is initialized from high energy to low energy. Initial sequencing is set by the one-electron physics, which is captured by the high frequency moment expansion of the Green’s function. This in turn already contains much of the information on the low energy correction. For instance in charge-transfer systems, the strength of correlations is set by the one-electron Hamiltonian (see work from Weber et al [46]). The hierarchy of energy scales, from high frequency towards low frequency, provides a ladder of many-body corrections that dresses the one-particle propagator [47, 48].

In this framework, the end of the prediction sequence is arbitrary, we can stop at any $n \geq 0$. The energy scale of interest is the low energy regime, therefore the sequence was chosen to end at $n = 0$. This choice of the end of sequence is an analogue to the end-of-sequence token or “<EOS>” in the natural language processing terminology (see for example the attention visualization section of Vaswani et al [29]).

Notwithstanding a shared numerical approach to large language models with the application of transformers, there exist further natural connections between the structure of the Matsubara GF and language. For instance, there is a strong hierarchy in the matsubara formalism, the large frequency limit obeys a constraint stemming from the fermionic statistics, and more generally high frequency moments obey sum rules (the second expansion term lies with the uncorrelated Hamiltonian). Moving from high frequency to the low frequency regime covers the range from free fermions to emergent quasi-particles at low energy. This structural hierarchy connects directly with an increasing level of quantum entanglement carried by the many-body states, not present at high frequency for the single particle physics, the entanglement being associated with the emergence of multi-determinant quantum states [49] or across impurities for multi-orbital systems [50].

These properties, which $G(i\omega_n)$ shares with natural language processing, allows the problem of correlated materials to be transcribed and tackled with the Trans-

former network. Lastly, the condition of causality of $G(i\omega_n)$ can be tested in straightforward manner, ensuring predicted solutions remain physical.

C. SCALINN Architecture

In this section, we consider an overview of the SCALINN architecture in terms of its various neural network blocks, where differences to the standard transformer architecture of Ref. 29 are particularly highlighted.

In natural language processing, traditional recurrent neural networks have a short memory, where the context gained from words at the start of a sentence could be lost when the model reaches the end of the sentence. The original Transformer network overcomes this difficulty by positional encoding, whereby the position of words in the sentence are supplemented upon the input word entries.

This method of positional encoding however, requires the input words to be cast into a vector format via word embedding techniques; corresponding to the meanings of various words encoded in vectors. Since Green's functions $G(i\omega_n)$ are sequences of scalars, instead of sequences of vectors, the original method of positional encoding would not be a viable solution to deal with the aforementioned memory issue. In SCALINN, we consider an explicit inclusion of the Matsubara frequency $\omega_n = (2n + 1)\pi/\beta$ of each Green's function sequence entry $G_l(i\omega_n)$ as positional encoding of the sequence.

Moreover, to reintroduce the representability of information afforded by word embedding in the original Transformer network, a multilayer perceptron (MLP) block is employed. This then leads to the encoder block, which is identical to the encoder block of the original network. This encoder block allows the network to perform self-attention, a method of computing the relevance and context between different entries within the input sequence. In total, information passes through this encoder block $n_{Encoder}$ number of times. In supplementary information A, we consider further the performance of the models with difference choices of $n_{Encoder}$ (see supplementary table 1).

Moving onto the decoder portion of the network, the input to the decoder is subject to the same Matsubara encoding, but is passed to another MLP block. In an effort to enhance the overall performance of the model, we integrate a masked multi-head self-attention (MHSA) mechanism in the decoder. This ensures that more significance ('attention') is placed on the input Green's function values around the Matsubara point of interest, which is achieved via a masking operation implemented by the \mathbf{M} matrix. The operation of each head is defined as follows:

$$\begin{aligned} \text{Attention}(Q, K, V) &= \text{softmax} \left(\frac{\mathbf{M}\mathbb{1} + QK^T}{\sqrt{d_k}} \right) \cdot V \\ \mathbf{M}_{ij}^{\text{RF-TGT}} &= \begin{cases} 0 & \text{if } i - \text{LB} < j < i + 1 \\ -\infty & \text{else} \end{cases} \\ \mathbf{M}_{ij}^{\text{SRC}} &= \begin{cases} 0 & \text{if } i - \text{LB} < j < i + 1 + \text{LF} \\ -\infty & \text{else} \end{cases} \end{aligned} \quad (12)$$

The queries, keys, and values - represented as Q, K, V , respectively - are the learned vector components in this MHSA. Here, d_k is defined as d_{model}/h , where d_{model} refers to the dimension of the model and h denotes the number of attention heads. Moreover, LF and LB, which signify lookforward and lookbackward respectively, are positive integers. These indicate the number of entries forwards / backwards in the sequence that the decoder can draw information from when considering the prediction of any entry. The matrices $\mathbf{M}^{\text{RF-TGT}}$ and \mathbf{M}^{SRC} are incorporated into the 'Right-Shifted Target Masked Multi-Head Self-Attention' (RF-TGT Masked MHSA) block and the 'Source Masked Multi-Head Self-Attention' (Source Masked MHSA) block respectively. Each attention head is then concatenated and projected to a dimension of d_{model} , following the methodology described in [29].

Different Green's functions are inputted to the Transformer decoder during training and run-time. During training, the entire target $G^{\text{ED}}(i\omega_n) \in \mathbb{R}^{N_\omega}$, $n \in [1, N_\omega]$ is already known. Following the MHSA mechanism, the dimensions of the query and keys are represented as $Q_{\text{RF-TGT}} \in \mathbb{R}^{N_\omega \times d_k}$ and $K_{\text{RF-TGT}} \in \mathbb{R}^{N_\omega \times d_k}$ respectively. Accordingly, a square-shaped subsequent mask, $\mathbf{M}^{\text{RF-TGT}} \in \mathbb{R}^{N_\omega \times N_\omega}$, is applied to predict the next Matsubara point in the sequence, while masking out the information of the target solution.

In contrast, the inputs to the Transformer encoder remain the same during both training and run-time, thus ensuring the output dimension of the Transformer encoder consistently remains $\mathbb{R}^{(N_\omega+1) \times d_{\text{model}}}$. Within the source masked MHSA layer, K and V are derived from the Transformer Encoder, resulting in $K_{\text{source}} \in \mathbb{R}^{(N_\omega+1) \times d_k}$ and $V_{\text{source}} \in \mathbb{R}^{(N_\omega+1) \times d_k}$. Concurrently, Q is sourced from the right-shifted target, leading to $Q_{\text{source}} \in \mathbb{R}^{N_\omega \times d_k}$. As a result, the source masked MHSA possesses the dimensions of $\mathbf{M}^{\text{src}} \in \mathbb{R}^{N_\omega \times (N_\omega+1)}$. This configuration effectively adjusts the attention scores within a scope that ranges between lookforward and lookbackward, enabling the model to adapt its focus according to the complexities of the input data.

The RF-TGT Masked MHSA blocks are responsible for performing self-attention with the decoder input, whereas the source MHSA block calculates self-attention between the encoder input and the decoder input. Generally, with a higher number of heads, the richness of information that can be learned in these multi-head self-attention blocks increases. This hyperparameter is var-

ied, and the performances of models with different number of heads, and different number of decoder blocks ($n_{Decoder}$) are listed in table A1.

Analogous to approximating Matsubara Green’s function with a Laurent expansion in powers of $(i\omega_n)^{-1}$, where Green’s function points at large values of $i\omega_n$ can be well understood through analytic commutator expansion for this tail, this Transformer model begins its sequence prediction at the *last* Matsubara point, $i\omega_{n=N_\omega-1}$. During prediction, the network decoder is ignorant to the $G^{ED}(i\omega_n)$ solution, and as such, an auxiliary Green’s function $G^{aux}(i\omega_n) \in \mathbb{R}^{N_\omega}$, $n \in [1, N_\omega]$ is iteratively constructed to fill the role of $G^{ED}(i\omega_n)$ as input to the decoder. We make the assumption that the highest frequency tail points of $G^{aux}(i\omega_n)$ are close to the input Green’s function, so that the sequence is initialized with $G^{aux}(i\omega_{n=N_\omega}) = G^{IPT}(i\omega_{n=N_\omega})$ for the ‘hybrid’ scheme. This is justified as the asymptotic behavior of the Matsubara Greens function at large values is entirely defined by the low-order perturbative expansion with respect to the interaction, which is described by IPT theory. To begin, $G^{aux}(i\omega_{n=N_\omega})$ are fed into the decoder, together with the full $G(i\omega_n^{input})$ sequence at the encoder, the network generates the next highest frequency point of $G^{aux}(i\omega_{n=N_\omega-1})$. Those high frequency $G^{aux}(i\omega_n)$ point are then kept and reintroduced to the decoder to approach low frequency points in G^{aux} , such that $G^{aux}(i\omega_{n=m+1})$ generates $G^{aux}(i\omega_{n=m})$ until the lowest frequency $G^{aux}(i\omega_{n=0})$ point is determined, resulting in the full predicted Green’s function. We denote this $\hat{G}(i\omega_n) \in \mathbb{R}^{N_\omega}$, $n \in [0, N_\omega - 1]$.

A important difference compared to the original Transformer model concerns the nature of the final output layer. In a language model, the outputs are the probabilities that inform which word would best fit the output sequence next. However, the output to our network is a prediction of the Green’s function — a sequence of continuous scalars instead of a discrete word — at the next Matsubara frequency point. As such, the softmax layer of the original model, which outputs normalized probabilities over a finite set (such as the case of word selection in the original work), is unsuited. The network therefore terminates with a linear layer without an activation

function.

DATA AVAILABILITY

An exemplary dataset can be found at <https://dx.doi.org/10.6084/m9.figshare.23144474>.

CODE AVAILABILITY

The code for SCALINN is available at <https://github.com/zelong-zhao/SCALINN>.

ACKNOWLEDGMENT

G.H.B. gratefully acknowledges support from the Air Force Office of Scientific Research under award number FA8655-22-1-7011. We are also grateful to the King’s Computational Research, Engineering and Technology Environment (CREATE) and UK Materials and Molecular Modelling Hub for computational resources, which is partially funded by EPSRC (EP/T022213/1, EP/W032260/1 and EP/P020194/1).

AUTHOR CONTRIBUTIONS

C.W., G.H.B, W.G., and Z.Z. conceived the project. C.W. and Z.Z build the database. W.G., H.L and Z.Z developed the Machine Learning model and trained the Transformer model. H.L and Z.Z. performed data analysis. All wrote the manuscript.

COMPETING INTERESTS

The authors declare no competing financial or non-financial interests.

CORRESPONDING AUTHOR

Correspondence to Weifeng Ge and Cedric Weber

-
- [1] A. Georges, G. Kotliar, W. Krauth, and M. J. Rozenberg, *Reviews of Modern Physics* **68**, 13 (1996).
 - [2] G. Kotliar, S. Y. Savrasov, K. Haule, V. S. Oudovenko, O. Parcollet, and C. Marianetti, *Reviews of Modern Physics* **78**, 865 (2006).
 - [3] E. Pavarini, A. Koch, Erik Lichtenstein, and D. Vollhardt, *DMFT: From Infinite Dimensions to Real Materials*, Vol. 4 (Forschungszentrum Jülich, 2018).
 - [4] G. Kotliar, S. Y. Savrasov, K. Haule, V. S. Oudovenko, O. Parcollet, and C. Marianetti, *Reviews of Modern Physics* **78**, 865 (2006).
 - [5] B. Amadon, *Physical Review B* **94**, 115148 (2016).
 - [6] K. Held, I. A. Nekrasov, N. Blümer, V. Anisimov, and D. Vollhardt, *International Journal of Modern Physics B* **15**, 2611 (2001).
 - [7] J. Hubbard, *Proc. Math. Phys. Eng. Sci. P ROY SOC A-MATH PHY* **276**, 238 (1963).
 - [8] H.-C. Jiang and T. P. Devereaux, *Science* **365**, 1424 (2019).
 - [9] M. Kheirhah, Z. Yan, Y. Nagai, and F. Marsiglio, *Phys. Rev. Lett.* **125**, 017001 (2020).

- [10] A. Foley, S. Verret, A.-M. S. Tremblay, and D. Sénéchal, *Phys. Rev. B* **99**, 184510 (2019).
- [11] J. Koepsell, J. Vijayan, P. Sompet, F. Grusdt, T. A. Hilker, E. Demler, G. Salomon, I. Bloch, and C. Gross, *Nature* **572**, 358 (2019).
- [12] P. T. Brown, D. Mitra, E. Guardado-Sanchez, R. Nourafkan, A. Reymbaut, C.-D. Hébert, S. Bergeron, A.-M. Tremblay, J. Kokalj, D. A. Huse, *et al.*, *Science* **363**, 379 (2019).
- [13] B. Yang, H. Sun, R. Ott, H.-Y. Wang, T. V. Zache, J. C. Halimeh, Z.-S. Yuan, P. Hauke, and J.-W. Pan, *Nature* **587**, 392 (2020).
- [14] C. Shao, E. V. Castro, S. Hu, and R. Mondaini, *Phys. Rev. B* **103**, 035125 (2021).
- [15] J. Fraxanet, D. González-Cuadra, T. Pfau, M. Lewenstein, T. Langen, and L. Barbiero, *Phys. Rev. Lett.* **128**, 043402 (2022).
- [16] D. González-Cuadra, A. Dauphin, P. R. Grzybowski, P. Wójcik, M. Lewenstein, and A. Bermudez, *Phys. Rev. B* **99**, 045139 (2019).
- [17] A. Georges, G. Kotliar, W. Krauth, and M. J. Rozenberg, *Rev. Mod. Phys.* **68**, 13 (1996).
- [18] A. Georges and G. Kotliar, *Phys. Rev. B* **45**, 6479 (1992).
- [19] P. W. Anderson, *Phys. Rev.* **124**, 41 (1961).
- [20] E. Gull, P. Werner, A. Millis, and M. Troyer, *Phys. Rev. B* **76**, 235123 (2007).
- [21] P. Werner and A. J. Millis, *Phys. Rev. B* **74**, 155107 (2006).
- [22] P. Werner, A. Comanac, L. De'Medici, M. Troyer, and A. J. Millis, *Phys. Rev. Lett.* **97**, 076405 (2006).
- [23] A. N. Rubtsov, V. V. Savkin, and A. I. Lichtenstein, *Phys. Rev. B* **72**, 035122 (2005).
- [24] M. Caffarel and W. Krauth, *Phys. Rev. Lett.* **72**, 1545 (1994).
- [25] M. Capone, L. de'Medici, and A. Georges, *Phys. Rev. B* **76**, 245116 (2007).
- [26] A. Liebsch and H. Ishida, *J. Phys. Condens. Matter* **24**, 053201 (2011).
- [27] D. P. Kingma and J. Ba, *arXiv 10.48550/arXiv.1412.6980* (2014).
- [28] Y. LeCun, Y. Bengio, and G. Hinton, *nature* **521**, 436 (2015).
- [29] A. Vaswani, N. Shazeer, N. Parmar, J. Uszkoreit, L. Jones, A. N. Gomez, Ł. Kaiser, and I. Polosukhin, *NeurIPS* **30**, 10.48550/arXiv.1706.03762 (2017).
- [30] V. Dunjko and H. J. Briegel, *Rep. Prog. Phys.* **81**, 074001 (2018).
- [31] G. Carleo, I. Cirac, K. Cranmer, L. Daudet, M. Schuld, N. Tishby, L. Vogt-Maranto, and L. Zdeborová, *Rev. Mod. Phys.* **91**, 045002 (2019).
- [32] J. Jumper, R. Evans, A. Pritzel, T. Green, M. Figurenov, O. Ronneberger, K. Tunyasuvunakool, R. Bates, A. Židek, A. Potapenko, *et al.*, *Nature* **596**, 583 (2021).
- [33] J. Kirkpatrick, B. McMorrow, D. H. Turban, A. L. Gaunt, J. S. Spencer, A. G. Matthews, A. Obika, L. Thiry, M. Fortunato, D. Pfau, *et al.*, *Science* **374**, 1385 (2021).
- [34] R. Fournier, L. Wang, O. V. Yazyev, and Q. Wu, *Phys. Rev. Lett.* **124**, 056401 (2020).
- [35] L.-F. Arsenault, A. Lopez-Bezanilla, O. A. von Lilienfeld, and A. J. Millis, *Phys. Rev. B* **90**, 155136 (2014).
- [36] E. Sheridan, C. Rhodes, F. Jamet, I. Rungger, and C. Weber, *Phys. Rev. B* **104**, 205120 (2021).
- [37] J. Rogers, T.-H. Lee, S. Pakdel, W. Xu, V. Dobrosavljevic, Y.-X. Yao, O. Christiansen, and N. Lanata, *Phys. Rev. Res.* **3**, 013101 (2021).
- [38] O. Parcollet, M. Ferrero, T. Ayrál, H. Hafermann, I. Krivenko, L. Messio, and P. Seth, *Comput. Phys. Commun.* **196**, 398 (2015).
- [39] A. H. Romero, D. C. Allan, B. Amadon, G. Antonius, T. Applencourt, L. Baguet, J. Bieder, F. Bottin, J. Bouchet, E. Bousquet, *et al.*, *The Journal of chemical physics* **152** (2020).
- [40] E. Plekhanov, P. Hasnip, V. Sacksteder, M. Probert, S. J. Clark, K. Refson, and C. Weber, *Physical Review B* **98**, 075129 (2018).
- [41] J. B. Rigo and A. K. Mitchell, *Physical Review B* **101**, 241105 (2020).
- [42] H. Kim, D. Kim, and D.-H. Kim, *New Physics: Sae Mulli* (2022).
- [43] E. J. Sturm, M. R. Carbone, D. Lu, A. Weichselbaum, and R. M. Konik, *Physical Review B* **103**, 245118 (2021).
- [44] C. Mejuto-Zaera, L. Zepeda-Núñez, M. Lindsey, N. Tubman, B. Whaley, and L. Lin, *Phys. Rev. B* **101**, 035143 (2020).
- [45] M. Granath and H. U. Strand, *Phys. Rev. B* **86**, 115111 (2012).
- [46] C. Weber, K. Haule, and G. Kotliar, *Nature Physics* **6**, 574 (2010).
- [47] K. Haule and K. Chen, *Scientific reports* **12**, 2294 (2022).
- [48] K. Chen and K. Haule, *Nature communications* **10**, 3725 (2019).
- [49] C. Weber, D. D. O'Regan, N. D. Hine, P. B. Littlewood, G. Kotliar, and M. C. Payne, *Physical review letters* **110**, 106402 (2013).
- [50] A. Baul, H. F. Fotsó, H. Terletska, J. Moreno, and K.-M. Tam, *arXiv preprint arXiv:2308.01392* (2023).
- [51] C. Weber, A. Amaricci, M. Capone, and P. Littlewood, *Phys. Rev. B* **86**, 115136 (2012).
- [52] A. Paszke, S. Gross, S. Chintala, G. Chanan, E. Yang, Z. DeVito, Z. Lin, A. Desmaison, L. Antiga, and A. Lerer, *openreview* (2017).

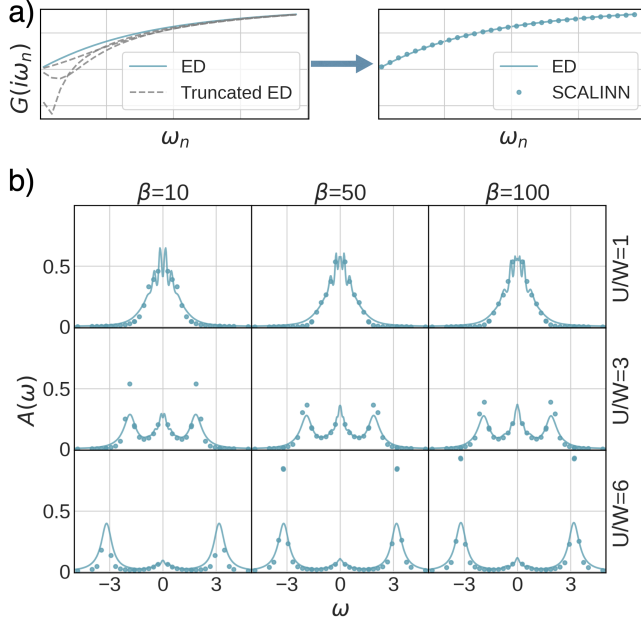


Fig. 1. **Representative SCALINN predictions for a test-set single impurity Anderson model with the truncated bath scheme.** In a), the desired (7-bath) exact diagonalization (ED) solution $G^{\text{ED}}(i\omega_n)$ is plotted as a blue line, and the three truncated (3-bath orbitals) $G^{\text{Trunc}}(i\omega_n)$ are plotted in dashed gray. These $G^{\text{Trunc}}(i\omega_n)$ act as inputs to the Transformer model to produce the SCALINN predictions $\hat{G}(i\omega_n)$, which are plotted as blue dots. In b), Padé analytic continuation obtains the predicted spectral function $A(\omega)$, shown here for three different values of inverse temperature β and on-site interaction U . Once again, the ED solution is plotted as blue lines, and the SCALINN predictions are plotted as blue dots.

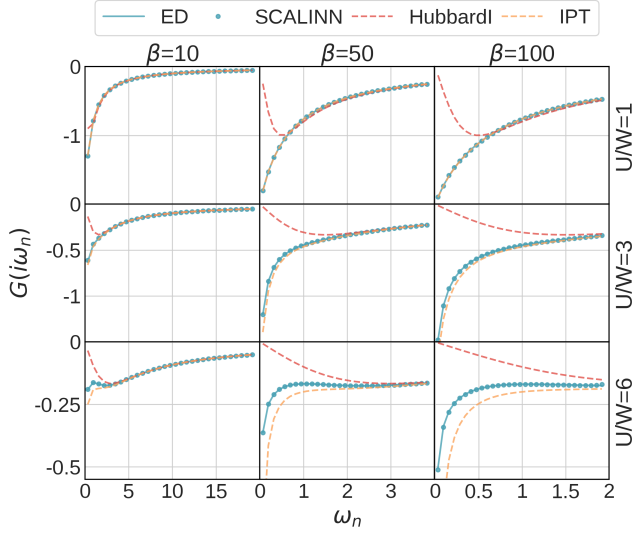


Fig. 2. **Representative SCALINN predictions for a test-set single impurity Anderson model with the HI+IPT hybrid scheme.** The Hubbard-I solution $G^{\text{HI}}(i\omega_n)$ (dashed red), the iterative perturbation theory (IPT) solver solution $G^{\text{IPT}}(i\omega_n)$ (dashed yellow), and the exact diagonalization (ED) target $G^{\text{ED}}(i\omega_n)$ (solid blue lines) are plotted alongside the SCALINN predictions from these input Green's functions (blue dots) at inverse temperature values $\beta = 10, 50, 100$ and at on-site interaction strength to bandwidth ratios $U/W = 1, 3, 6$.

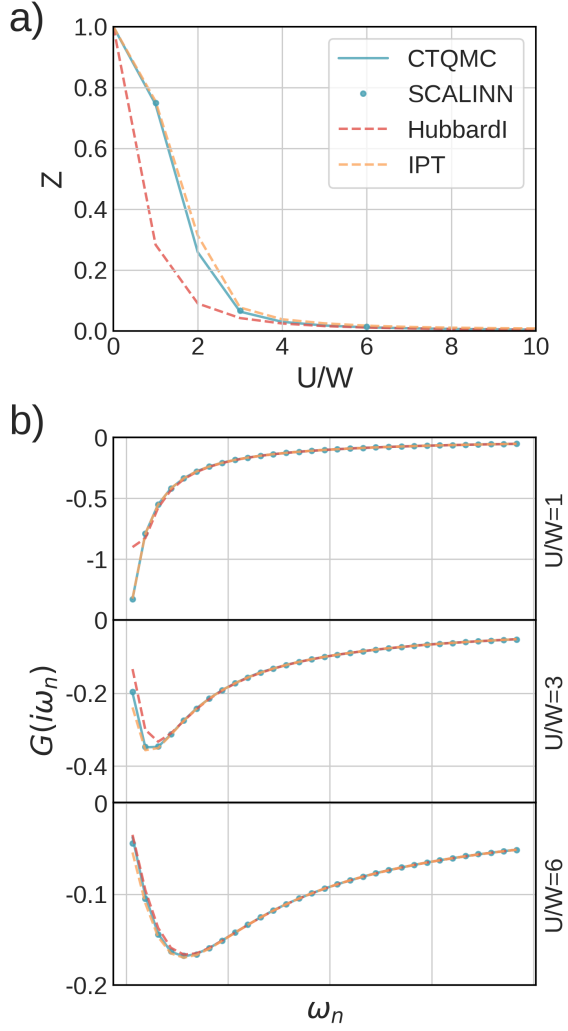


Fig. 3. **Converged self-consistent dynamical mean field theory (DMFT) results on the Bethe Hubbard lattice for different solvers: iterative perturbation theory (IPT), Hubbard-I, SCALINN and continuous time quantum Monte Carlo CTQMC.** a) Quasi-particle weight Z b) Imaginary part of Matsubara Green's functions. DMFT is converged at inverse temperature $\beta = 10$ for the continuous hybridization of Eq. 1 without bath discretization error, with the IPT and Hubbard-I solutions at each iteration used as input for the SCALINN solver approach.

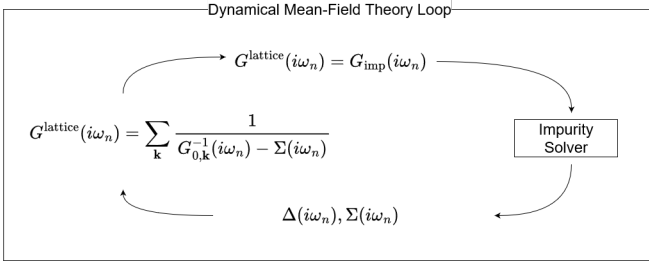


Fig. 4. Schematic diagram of the dynamical mean field theory (DMFT) iterative loop. The lattice Green's function $G^{\text{lattice}}(i\omega_n)$ obtained from summing over all the momentum dependent Green's functions of the system, the impurity Green's function $G_{\text{imp}}(i\omega_n)$ is then defined to equate this lattice Green's function. The role of the impurity solver is to calculate hybridization $\Delta(i\omega_n)$ and self-energy $\Sigma(i\omega_n)$ functions that such that $G_{\text{imp}}(i\omega_n)$ and $G^{\text{lattice}}(i\omega_n)$ match. The new $G^{\text{lattice}}(i\omega_n)$ is then calculated from all momentum independent, non-interacting Green's functions $G_{0,\mathbf{k}}(i\omega_n)$ through the Dyson equation.

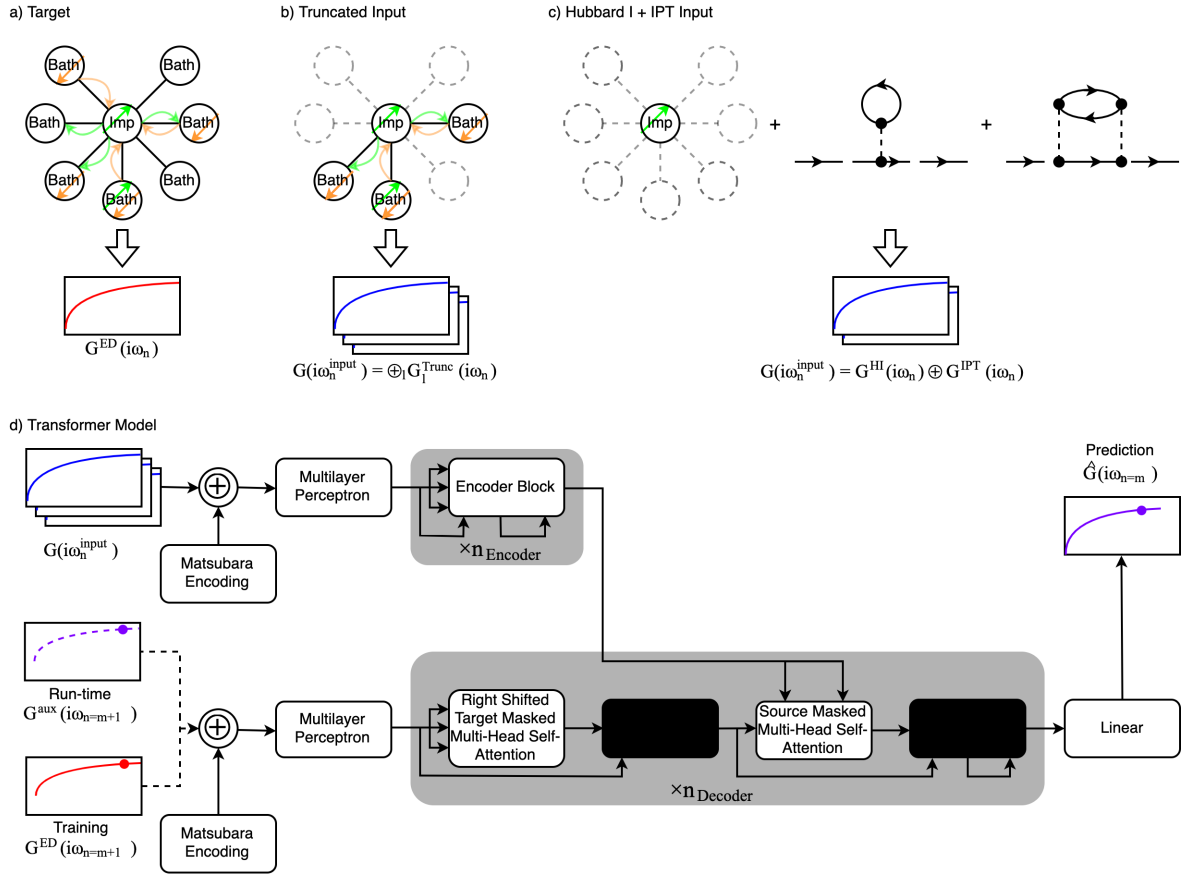


Fig. 5. **Illustrations of the target, inputs and structure of the Transformer model.** a) target output from the model, trained on exact diagonalization (ED) Green's functions. Quantum fluctuations between spin up and spin down electrons between the correlated impurity and bath are illustrated with green and orange arrows respectively, while hybridizations between impurity and bath are depicted as curved arrows. ED green's functions $G^{\text{ED}}(i\omega_n)$ are shown in red, and act as targets of the Transformer model. b) The truncated scheme input Green's functions, where a number of bath orbitals are discarded from the full single impurity Anderson model for its solution. Multiple ED Green's functions are calculated per one target $G^{\text{ED}}(i\omega_n)$, each with a different combination of removed bath orbitals c) The Hubbard I (HI)+ iperative perturbation theory (IPT) hybrid scheme, where a Hubbard-I Green's function and IPT Green's function is used as input. These Green's functions are stacked to form the input to the model. d) The Transformer model architecture, where neural network blocks taken from [29] are used as the encoder block and blacked-out blocks.